IEEE Access
Multidisciplinary ⋮ Rapid Review ⋮ Open Access Journal

Received September 25, 2021, accepted October 14, 2021, date of publication October 21, 2021, date of current version October 26, 2021.

*Digital Object Identifier 10.1109/ACCESS.2021.3121072*

# Residual Current Detection Method Based on Variational Modal Decomposition and Dynamic Fuzzy Neural Network

**XIANGKE ZHANG, ZHENMING LIU, YAJING WANG, ZHENHAI DOU, GUOLIANG ZHAI, AND QINQIN WEI**

College of Electrical and Electronic Engineering, Shandong University of Technology, Zibo, Shandong 255049, China

Corresponding author: Yajing Wang (wangyajing@sdut.edu.cn)

This work was supported by the Shandong University of Technology and the Zibo City Integration Development Project under Grant 2019ZBXC011 and Grant 2019ZBXC498.

**ABSTRACT** To further improve the detection ability of residual current in low-voltage distribution networks, an adaptive residual current detection method based on variational mode decomposition (VMD) and dynamic fuzzy neural network (DFNN) is proposed. First, using the general $K$-value selection method of VMD proposed in this study, the residual current signal is decomposed into $K$ intrinsic mode functions (IMFs). By introducing the cross-correlation coefficient $R$ and the time-domain energy entropy ratio $E$ as two classification indexes, IMFs are divided into three categories: effective IMFs, noise IMFs and aliasing IMFs. Then, the aliasing IMFs are denoised by recursive least squares (RLS), and the denoised IMFs are superimposed with the effective IMFs to obtain the reconstructed signal. Finally, the dynamic fuzzy neural network (DFNN) is adjusted by the minimum output method to achieve the detection of the reconstructed residual current signal, and the network is used to predict the residual current according to the detection results. The detection results of the simulation and measured data show that the proposed algorithm has high detection accuracy and is superior to the wavelet neural network, empirical mode decomposition-thresholding, and wavelet entropy-auto encoder-back propagation neural network methods in terms of mean square error, goodness of fit and running time. This method provides a reference for further research on new adaptive residual current protection devices.

**INDEX TERMS** Adaptive signal processing, electrical fault detection, fuzzy neural networks, residual current, variational modal decomposition.

## I. INTRODUCTION

With the widespread application of electrical equipment, it has been difficult for traditional residual current devices (RCD) has been difficult to meet the complex electrical environment and the requirements of the public for daily electrical safety. Many electric shock accidents and electrical fires are caused by the insufficient detection capability of the RCD. When the human body accidentally contacts the charged conductor, a fast and correct action of the RCD can prevent electric shock accidents from occurring. Most electrical fires are caused by electric arcs generated from short-circuit faults. Impacted by impedance, if the short-circuit current does not reach the overcurrent action value of the RCD, the electric arc will exist for a long time causing high temperatures and fires. If the RCD has a higher detection accuracy and speed, it can quickly and correctly cut off the power to prevent electric shock accidents or electrical fires. Therefore, further improvement of the detection ability of the residual current is the development direction of the RCD. However, the residual current signal is a weak singular signal and has serious noise interference, therefore, it is necessary to achieve fast and accurate residual current detection while ensuring the effectiveness of the detection signal. Accurate extraction of the effective components from the residual current signal is the basis for guaranteeing the quick and correct action of the RCD. Therefore, we further studied a method to improve the residual current detection ability of

The associate editor coordinating the review of this manuscript and approving it for publication was Hao Shen.

RCD. At present, many scholars have proposed a variety of methods to improve the accuracy and speed of residual current detection [1]–[5].

With the development of modern signal processing technology, some related technologies have been applied to residual current detection, such as wavelet analysis, neural networks and empirical mode decomposition (EMD). The traditional RCD only acts according to the peak current, which easily leads to false action and refusing action, and these modern signal processing methods overcome the shortcomings of traditional RCD and further improve the reliability of RCD. For example, J. Wang and H. Guan proposed an EMD-thresholding (EMD-T) residual current detection model based on the Hilbert-Huang transform, which can extract the residual current more effectively than the traditional FIR filtering method [6], [7]. C. Li proposed the combination of wavelet transform (WT) and back propagation neural network (BPNN) to preprocess the signal with multiscale wavelets, and then used the processed signal as a sample for detection and analysis by BPNN [8]. S. Wu proposed a residual current detection model based on wavelet entropy and an Auto Encoder to extract feature information, and classification by BPNN (WE-AE-BP) to achieve the detection and classification process of residual current [9]. X. Han proposed an adaptive residual current detection model by optimizing the parameters of recursive least squares (RLS) and SVM [10]. Although these methods improve detection accuracy of residual current to varying degrees, they also have some shortcomings. For example, EMD is prone to produce endpoint effects, and the existence of noise will cause EMD to produce mode aliasing and false components, which will reduce the detection accuracy [11]. The WT needs to set the fundamental wave, decomposition layer, threshold, and threshold function in advance, which reduces the adaptability of the algorithm [12]. The BPNN has a long training time, and the parameter settings for the number of neurons and network layers need to be adjusted several times. In practical applications, the structure and parameters of neural networks will change uncontrollably. To solve this problem, many scholars have proposed neural network control methods, for example, S. Lin proposed the use of Weibull distribution to represent the residence time of each mode in a neural network, and designed mode-dependent estimator gains to track the state of the original system, so that the states of the error system satisfying a dissipative performance index converge to zero asymptotically [13]. J. Wang proposed an adaptive pinning control strategy in fuzzy coupled neural networks, which can adjust the fuzzy neural network adaptively by a few nodes [14]. For the Takagi-Sugeno fuzzy model, J. Wang proposed a matrix transformation method to deal with the double summation inequality with fuzzy weight functions, which has good stability [15]. In summary, these methods have optimized the structure and parameters of neural networks, and have achieved good results in different applications.

In contrast, the fuzzy rules function and neural network structure of a dynamic fuzzy neural network (DFNN) are not set in advance, but constantly adjust the corresponding fuzzy rules function in the learning process. The DFNN has lower requirements for initial parameter setting and better adaptability, therefore, we use the minimum output method to construct the DFNN to detect the residual current. However, in practical applications, the residual current signal usually contains noise, which can cause serious interference to the detection. Considering that VMD is sensitive to noise and overcomes the shortcomings of EMD, such as the endpoint effect and false component, the VMD is used to preprocess the residual current signal [16]. However, the number of VMD decomposition levels $K$ needs to be determined in advance, so we proposed the concept and selection method of the general $K$-value. This method can preliminarily determine the $K$-value of the residual current for a certain fault type, which avoids a large number of calculations caused by seeking the optimal $K$-value and improving the adaptive ability of VMD. To solve the problem of inaccurate information extraction caused by the aliasing effect that may exist in VMD, we proposed a classification method of IMFs with cross-correlation coefficient $R$ and time domain energy entropy ratio $E$ as the classification indexes [17]–[19]. This method can divide IMFs into three categories: effective IMFs, aliasing IMFs, and noise IMFs. For the aliasing IMFs, the recursive least-squares (RLS) method is used for secondary noise reduction, and the denoised aliasing IMFs are superposed with the effective IMFs. Thus, an effective information extraction method for RE-RLS-VMD is proposed. On this basis, RE-RLS-VMD is combined with DFNN, and an adaptive residual current detection method (RE-RLS-VMD-DFNN) is constructed, which has a faster detection speed and higher accuracy. The results of the measured and simulated signals show that this method can detect the residual current signal faster and more accurately than the wavelet neural network (WNN), empirical mode decomposition threshold (EMD-T), and wavelet entropy-automatic encoder-back propagation neural network (WE-AE-BP) methods in different fault environments.

## EXPLANATION OF THE SYMBOLS

| Symbols | Meaning |
|---|---|
| $x_i$ | The sampling point of the residual current signal. |
| $G_{ij}$ | The $j$th membership function of $x_i$. |
| $c_{ij}$ | The $j$th Gaussian function center of $x_i$. |
| $\sigma_j$ | The $j$th Gaussian function width of $x_i$. |
| $\boldsymbol{X}$ | The $\boldsymbol{X} = (x_1, x_2, \ldots, x_n)$. |
| $\boldsymbol{C}_j$ | The A is the $j$th RBF unit center, $\boldsymbol{C}_j = (c_{1j}, \ldots, c_{nj})$ |
| $d_i(j)$ | The accommodation boundary of $j$th Gaussian function |
| $k_d$ | The effective radius, $k_d = 0.2$. |
| $u$ | The number of Gaussian membership functions. |
| $n$ | The number of input. |

| | |
|---|---|
| $\varphi_j$ | The $j$th fuzzy rule. |
| $\|e_i\|$ | The system error. |
| $k_e$ | The expected accuracy error, $k_e = 0.0015$. |
| $d_i$ | The expected output of the $i$th input signal $x_i$. |
| $y_i$ | The actual output of the current network structure. |
| $\phi_i$ | The $i$th normalization layer node. |
| $\varpi_k$ | The $\varpi_k$ is connection weight of $k$th rule, $k = 1, 2, \ldots, u$. |
| $D_{(n\times v)}$ | The expectation matrix. |
| $err_i$ | The error reduction rate. |
| $X$ | The $i$th column of $X$ corresponds to the error reduction rate for the $i$th fuzzy rule. |
| $\eta_i$ | The importance of the $i$th fuzzy rule. |
| $k_{err}$ | The threshold value for the importance of fuzzy rules, $k_{err} = 0.0025$. |
| $u_k(t)$ | The amplitude of the $k$th IMF. |
| $\omega_k(t)$ | The center frequency of the $k$th IMF. |
| $\varphi_k(t)$ | The phase of the $k$th IMF component, $\varphi_k(t) \geq 0$. |
| $A_k(t)$ | the envelope of the $k$th IMF component, $A_k(t) \geq 0$. |
| $\delta(t)$ | The pulse function. |
| $K$ | The number of IMFs decomposed by VMD. |
| $j$ | The imaginary unit. |
| $*$ | The denotes convolution. |
| $\alpha$ | The secondary penalty item. |
| $\lambda$ | The Lagrangian multiplier. |
| $\hat{u}_k^{n+1}(\omega)$ | The Fourier transform of $u_k^{n+1}(t)$. |
| $\omega_k^{n+1}(\omega)$ | The Fourier transform of $\omega_k^{n+1}(t)$. |
| $\gamma$ | The noise margin, usually $\gamma = 0$. |
| $\zeta$ | The convergence accuracy, $\zeta < 1e^{-7}$ |
| SNR | The signal-to-noise ratio. |
| $R$ | The Cross-Correlation coefficient. |
| $E_k$ | The time-domain energy entropy ratio of $k$th IMF. |
| $e(t)$ | The estimation error function, represents the difference between the expected and output residual current signal. |
| $W(t)$ | The optimal weight vector. |
| $k(t)$ | The gain vector. |
| $P(t)$ | The minimum-cost function. |
| $\Delta$ | The forgetting factor of RLS. |
| $x(t)$ | The amplitude of original signal at each sampling point. |
| $IMF_k(t)$ | The $k$th IMF and $t$ is the amplitude of each sample point of the $k$th IMF. |
| $x'(t)$ | The amplitude of reconstructed signal. |
| $Cov(A, B)$ | The covariance of A and B. |
| $Var(A, B)$ | The variance between A and B. |
| $y(t)$ | The final result of DFNN output. |
| $\hat{u}_i(\omega)$ | The Fourier transform of $u_i(t)$. |
| $\hat{\lambda}(\omega)$ | The Fourier transform of $\lambda(t)$. |

## II. PRINCIPLE OF THE DFNN

The DFNN is an optimized neural network based on a fuzzy inference system, which combines the advantages of a fuzzy system for fast processing of complex nonlinear signals and the strong self-learning ability of the neural network [20]. It can achieve fast detection of nonlinear signals such as residual current, while ensuring detection accuracy.

### A. STRUCTURE OF THE DFNN

The biggest difference between the DFNN and traditional neural networks is that the network structure of the DFNN is not set in advance [21]. Before inputting the first data, the rule function of the neural network and the number of neurons in each layer were zero. With the continuous input of data, the fuzzy rule function was dynamically adjusted using the minimum output method. The basic structure of the DFNN is illustrated in Fig. 1.

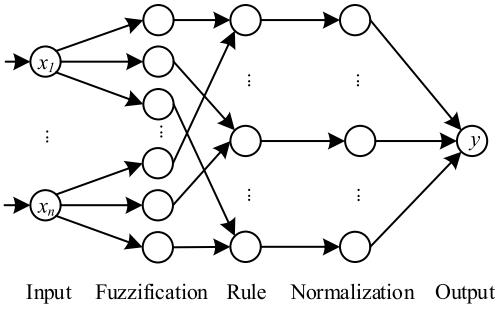


**FIGURE 1.** The basic structure of DFNN.

As shown in Fig. 1, the DFNN structure is divided into five layers, where the first layer is the input layer, and each node represents a sampling point $x_i$ of the residual current signal. The second layer is the fuzzification layer, and each node represents a Gaussian membership function, as shown in (1).

$$G_{ij}(x_i) = \exp[-\frac{(x_i - c_{ij})^2}{\sigma_j^2}] \; i = 1, 2, \ldots, n; j = 1, 2, \ldots, u \tag{1}$$

The coverage of the Gaussian membership function is called accommodation boundary $d_i(j)$. To simplify the network structure, a new Gaussian membership function is not allowed when the signal is within the accommodation boundary, otherwise, it is allowed. The formula for accommodating boundary $d_i(j)$ is given by (2).

$$d_i(j) = \|x_i - c_{ij}\| \tag{2}$$

When the signal exceeds the effective radius $k_d$, that is $d_{\min} = \arg\min(d_i(j)) > k_d$, the new Gaussian membership function is added.

The third layer is the rule layer, also known as the T-norm layer, where each node represents a fuzzy rule, as shown

in (3).

$$\varphi_j = \exp\left[-\frac{\sum_{i=1}^{n}(x_i - c_{ij})^2}{\sigma_j^2}\right] = \exp\left[-\frac{\|\boldsymbol{X} - \boldsymbol{C}_j\|}{\sigma_j^2}\right] \quad (3)$$

The system error $||e_i||$ was used to determine whether the new fuzzy rule could be added. When $||e_i||$ is greater than the expected accuracy error $k_e$, the new fuzzy rule $\varphi_j$ can be added to the rule layer. As shown in (4).

$$\|e_i\| = \|d_i - y_i\| \quad (4)$$

The fourth layer is the normalization layer, where the number of nodes in the normalization layer is the same as the number of nodes in the rule layer. The output of the $i$th normalization layer node is given by (5).

$$\phi_i = \frac{\varphi_i}{\sum_{k=1}^{u}\varphi_k} \quad (5)$$

The fifth layer is the output layer, which is the output of all the input residual current signals after processing. As shown in (6).

$$y(\boldsymbol{X}) = \sum_{k=1}^{u}\varpi_k\phi_k \quad (6)$$

### B. ELIMINATION OF DFNN FUZZY RULE

In traditional fuzzy neural networks, fuzzy rule functions always exist after generation. Some fuzzy rule functions will be invalid and become redundant fuzzy rule functions, and the existence of redundant fuzzy rule functions will lead to an increase in computation. To overcome this shortcoming, it is necessary to eliminate the redundant function in DFNN, so that the structure of the fuzzy neural network is more compact and the operation speed is improved. The methods of eliminating redundant fuzzy functions mainly include sensitivity calculation, weight subtraction, competitive learning, and the minimum output method. The sensitivity calculation method eliminates the fuzzy rule functions with low sensitivity by calculating the sensitivity of each fuzzy rule function to the global objective function. However, after eliminating a fuzzy rule function, the remaining fuzzy rule functions need to be recalculated, which leads to a large number of calculations. The weight subtraction method is applied to the BPNN by adding penalty terms to the objective function, which causes the weight coefficient of the unimportant function to gradually decay to zero. The disadvantage is that the weight coefficient decays to zero for a long time, and the function with the highest weight coefficient is not necessarily the most important. Competitive learning retains highly relevant fuzzy rules by calculating the relationship between the input and output of the fuzzy rules. However, this method does not consider the relationship between fuzzy rule functions, therefore, the results are not optimal. The minimum output method used in this study is to transform the expectation matrix into a set of orthogonal basis vectors by QR decomposition and calculate the contribution of each basis vector to the desired output energy value. Then, the importance of each fuzzy rule function is determined by the error reduction rate, the fuzzy rule functions are eliminated below the threshold, and the dynamic adjustment of the fuzzy neural network is realized. Compared with other methods, the minimum output method has obvious physical significance, stable numerical calculation and less calculation, which can ensure the effectiveness of the fuzzy rule function. Therefore, we chose the minimum output method to eliminate redundant fuzzy rule functions in the DFNN. The steps are as follows.

1) The QR decomposition is performed on expectation matrix $D_{(n\times v)}$. As shown in (7).

$$D = QR \quad (7)$$

where $Q = (q_1, q_2, \ldots, q_v)_{(n\times v)}$, $R_{(v\times v)}$ is the upper triangular matrix.

2) The error reduction rate $err_i$ is shown in (8).

$$err_i = \frac{(q_i^T D)^2}{q_i^T q_i D^T D} \quad (8)$$

3) The matrix $X = (\xi_1, \xi_2, \ldots, \xi_v)$ is composed of $err_i$, whose order is determined by the subscript of $err_i$. The $i$th column of $X$ corresponds to the error reduction rate for the $i$th rule.

4) The value of $\eta_i$ is representing the importance of the $i$th fuzzy rule function. As shown in (9).

$$\eta_i = \sqrt{\frac{\xi_i^T \xi_i}{v+1}} \quad (9)$$

5) When $\eta_i < k_{err}$, the $i$th rule will be eliminated.

By eliminating the fuzzy rule functions, the parameters and structure of the network can be adjusted in real time, which further enhances the adaptiveness of the neural network and can process nonlinear signals in real time. Compared with the traditional neural network, the DFNN has a higher detection accuracy and speed. Therefore, the DFNN constructed by the minimum output method was used to the detect residual current signal in this study.

## III. VMD NOISE REDUCTION

In practical applications, residual current signals usually contain strong noise, which significantly reduces the detection accuracy and increases the running time. Therefore, it is necessary to preprocess the measured residual current signal. VMD is an adaptive signal processing method that iteratively search for variational models, and has been widely used for signal denoising and feature extraction in recent years [22], [23]. In this study, VMD was used to preprocess the residual current signal. For VMD denoising, S. Li used the cross-correlation coefficient of each IMF and the original signal to screen the effective components [24], and X. Chen extracted the effective information according to the

permutation entropy of each IMF to achieve signal denoising [25]. However, for weak signals, such as the residual current, it is difficult to effectively extract all the effective components based on a single indicator only. Therefore, we propose an information extraction method based on the RE-RLS-VMD. First, according to the general $K$-value method proposed in this study, the residual current is decomposed into $K$ IMFs by VMD. Second, according to the classification indexes of the cross-correlation coefficient $R$ and time-domain energy entropy ratio $E$, the IMFs are divided into three categories: effective IMFs, aliasing IMFs, and noise IMFs. Then, the aliasing IMFs are further denoised by RLS and the denoised aliasing IMFs are superimposed with the effective IMF to obtain the reconstructed residual current signal. This method can effectively extract information and improve the denoising ability of VMD.

### A. PRINCIPLE OF THE VMD

The VMD decomposes the residual current signal containing noise into $k$ IMFs. Moreover, the amplitude and center frequency of each IMF are redefined to ensure that each IMF has an independent center frequency, as shown in (10).

$$u_k(t) = A_k(t)\cos(\varphi_k(t)) \tag{10}$$

To ensure that the IMFs are all modal components with a finite bandwidth of the central frequency, the sum of the estimated bandwidths of each IMF is minimized. The constraint condition of the VMD is that the sum of all IMFs is equal to the original signal, as shown in (11).

$$\begin{cases} \min\limits_{\{u_k(t)\},\{\omega_k(t)\}} \left\{ \sum\limits_k \left\| \partial_t \left[ \left(\delta(t) + j/\pi t\right) * u_k(t) \right] e^{-j\omega_k t} \right\|_2^2 \right\} \\ s.t. \sum\limits_{k=1}^{K} u_k(t) = x(t) k = 1, 2, \ldots, K \end{cases} \tag{11}$$

To reduce the constraint conditions and obtain the optimal solution of the amplitude and center frequency, the secondary penalty item $\alpha$ and the Lagrangian operator $\lambda$ are introduced when reconstructing the constraint conditions. The Lagrangian strengthening matrix is given by (12).

$$\begin{aligned} &L(u_k(t), \omega_k(t), \lambda) \\ &= \alpha \sum_k \left\| \partial_t \left[ \left(\delta(t) + j/\pi t\right) * u_k(t) \right] e^{-j\omega_k t} \right\|_2^2 \\ &\quad + \left\| x(t) - \sum_k u_k(t) \right\|_2^2 + \left\langle \lambda(t), x(t) - \sum_k u_k(t) \right\rangle \end{aligned} \tag{12}$$

Steps of the VMD algorithm:

1) Initialize $u_k^1(t)$, $\omega_k^1(t)$, $\lambda$, make $n = 0$, and determine the number of decompositions $K$.
2) Let $n = n+1$ and $k = 0$ to start the iterative computation.
3) Let $k = k+1$ and $k \le K$. According to (13), updates $u_k^n(t)$ and $\omega_k^n(t)$ respectively.

$$\begin{cases} \hat{u}_k^{n+1}(\omega) = \dfrac{\hat{x}(\omega) - \sum_{i \ne k} \hat{u}_i(\omega) + \hat{\lambda}(\omega)/2}{1 + 2\alpha(\omega - \omega_k)^2} \\ \omega_k^{n+1}(\omega) = \dfrac{\int_0^\infty \omega \left| \hat{u}_k^{n+1}(\omega) \right|^2 d\omega}{\int_0^\infty \left| \hat{u}_k^{n+1}(\omega) \right|^2 d\omega} \end{cases} \tag{13}$$

4) Update the Lagrangian operator:

$$\hat{\lambda}^{n+1}(\omega) = \hat{\lambda}^n(\omega) + \gamma \left[ \hat{x}(\omega) - \sum_k \hat{u}^{n+1}(\omega) \right] \tag{14}$$

5) When $k = K$, the iteration is terminated according to convergence accuracy $\zeta$. If the termination condition is satisfied, the iteration is stopped; otherwise, it is transferred to Step 2. The calculation formula for convergence accuracy is shown in (14).

$$\zeta = \sum_k \frac{\left\| \hat{u}_k^{n+1}(t) - \hat{u}_k^n(t) \right\|_2^2}{\left\| \hat{u}_k^n(t) \right\|_2^2} < 1e^{-7} \tag{15}$$

Through the above process, VMD decomposes the residual current signal into $K$ IMF components that satisfy the convergence accuracy.

### B. SELECTION OF DECOMPOSITION LEVEL K

In the VMD algorithm, the number of IMFs depends on the decomposition level $K$. The improper selection of the $K$-value directly affects the accuracy of the reconstructed signal. If the $K$-value is too small, the signal will be under-decomposed to cause aliasing. If the $K$-value is too large, it will lead to over-decomposition of the signal and jump in the center frequency of the IMF, both of which will have adverse effects on signal reconstruction [26]. Y. Shi proposed a method for optimizing the $K$-value of VMD. The $K$-value increases from 1, when the instantaneous frequency mean curve of the IMFs changes smoothly, the $K$-value is determined as the optimal $K$-value [27]. However, this method is equivalent to performing multiple VMD decompositions, which are computationally intensive and have a long running time. Q. Ge proposed using decomposition levels of EMD to determine the optimal $K$-value of VMD [28]; however, in practical applications, the number of IMFs decomposed by EMD will change with the noise, and it is easy to produce false components. J. Ding proposed an adaptive genetic optimization algorithm to find the optimal $K$-value of VMD, but the genetic algorithm usually needs a priori basis and easily falls into a local optimum [29].

To solve the problem of selecting the $K$-value, we put forward the concept and selection method of general $K$-value. For different fault types, by studying the influence of different $K$ values on the signal-to-noise ratios (SNR) of the reconstructed signal and the cross-correlation coefficient $R$ between the reconstructed signal and the original signal, the $K$ value with the highest average value of SNR and $R$

is selected as the general $K$-value. According to the general $K$-value, the specific fault-type signal is decomposed into $K$ IMFs by VMD. After classifying and processing the IMFs, the preprocessing of the fault signals was completed.

Taking the residual current signal of a single direct grounding fault occurring in a wetland environment as an example, through analysis of the measured data, the general $K$-value in this fault is determined. The specific process is as follows:

1) The residual current signals are collected by an oscilloscope, and the collected residual current signal is taken as the original signal. To collect clear experimental data, a high-resolution sampling mode was adopted for the acquisition.
2) The data collected in the high-resolution sampling mode were automatically filtered by the oscilloscope. To study the influence of noise and general $K$-value, different Gaussian white noises were added to the original signal to simulate the measured residual current signal without oscilloscope filtering. The SNR was 10 dB, 15 dB, and 25 dB, respectively. The formula for calculating the SNR is shown in (16).

$$SNR = 20\log_{10}(\frac{A_{signal}}{A_{noise}}) \tag{16}$$

where $A$ represents the signal amplitude.
3) VMD with different $K$ values is used to denoise the signal and remove the IMFs of the high-frequency components. Based on a large number of data processing results, $K$ generally takes three, four, five, and six.
4) To describe the denoising effect and reconstruction ability of VMD under different $K$ values, the SNR of the reconstructed signal and the $R$ between the reconstructed signal and the original signal are calculated respectively, as shown in Table 1. The calculation formula for $R$ is given in (17).

$$R(x(t), x'(t)) = \frac{Cov(x(t), x'(t))}{\sqrt{Var\,[x(t)]\,Var\,|x'(t)|}} \tag{17}$$

5) Based on the average values of the SNR and $R$, the general $K$-value was selected. It can meet the requirements of processing signals of specific fault types, as shown in Table 2.

**TABLE 1. Comparison of denoising effect of VMD with different K values under different SNR.**

| The SNR of original signal/dB | Indicators | $K$=3 | $K$=4 | $K$=5 | $K$=6 |
|---|---|---|---|---|---|
| 10 | SNR | 19.698 | 23.147 | 26.760 | 23.266 |
| | $R$ | 0.8743 | 0.8538 | 0.8846 | 0.8635 |
| 15 | SNR | 27.717 | 31.489 | 30.164 | 28.422 |
| | $R$ | 0.8953 | 0.9038 | 0.9174 | 0.8935 |
| 25 | SNR | 32.125 | 29.582 | 28.532 | 28.847 |
| | $R$ | 0.9263 | 0.9042 | 0.9184 | 0.8948 |

**TABLE 2. Average of VMD under different K values.**

| Average | $K$=3 | $K$=4 | $K$=5 | $K$=6 |
|---|---|---|---|---|
| SNR/dB | 26.513 | 28.073 | 28.495 | 26.845 |
| $R$ | 0.8986 | 0.8873 | 0.9068 | 0.8839 |

From Table 1, when the SNR of the original signal is 10 dB, the optimal $K$-value is 5. When the SNR is 15 dB, the optimal $K$-value is 4. When the SNR is 25 dB, the optimal $K$-value is 3. Therefore, the optimal $K$-value of the VMD in different SNR environments is uncertain. Therefore, we proposed to choose the general $K$-value based on the average of the SNR and $R$.

It can be seen from Table 2 that when $K = 5$, the average values of SNR and $R$ are higher than those of the other $K$ values. Therefore, the general $K$-value of the VMD is determined to be 5 for this fault type. The general $K$-values for other fault types were also selected through the above steps.

### C. INFORMATION EXTRACTION OF RE-RLS-VMD

However, the general $K$-value is not necessarily the optimal $K$-value. To further improve the accuracy of information extraction, we introduced the cross-correlation coefficient $R$ and the time-domain energy entropy ratio $E$ as classification indexes, and classified the IMF generated by VMD into effective IMF, noise IMF, and aliasing IMF, for which the aliasing IMF is subjected to secondary noise reduction by RLS.

To distinguish the effective IMFs from the IMFs, $x'(t)$ in (17) is replaced by $\mathrm{IMF}_k(t)$. The $R$ value between the original signal and each IMF was calculated as a classification index. When $R \geq 0.8$, it can be regarded as a high correlation between the two variables, defined as an effective IMF.

Then, to further distinguish the noise IMFs and aliasing IMFs, the time-domain energy entropy ratio $E_k$ is used to determine whether the IMF is an aliasing IMF. The calculation formula of $E_k$ is shown in (18).

$$E_k = \left(\frac{\int_0^t |\mathrm{IMF}_k(t)|^2 dt}{\int_0^t |x(t)|^2 dt}\right) \quad k = 1, 2, \ldots, K \tag{18}$$

After intensive analysis of the processing results of residual current signals, we found that the IMF components with $E_k \geq 10\%$ can contain the most effective components and a small amount of noise, and the IMF components with $E_k < 10\%$ are mostly high-frequency noise components. Therefore, when the IMFs with $E_k \geq 10\%$ and R $< 0.8$ are treated as aliasing IMFs, the residual current signal with noise can be well reconstructed after RE-RLS-VMD-DFNN processing. Therefore, when the $E$ of the IMF is greater than 10 % and $R$ is less than 0.8, it is considered to be the aliasing IMF.

Because effective information is also present in the aliasing IMFs, it is necessary to further denoise the aliasing IMFs to extract the effective information more fully. Considering that RLS has the advantages of simple calculation, good

convergence speed and adaptive adjustment parameters [30], RLS is used to denoise the aliasing IMFs in this study.

RLS introduces the estimation error function $e(t)$ to update the optimal weight vector $W(t)$ based on the least-squares method, as shown in (19).

$$W(t) = W(t-1) + k(t)e(t) \tag{19}$$

The constraint condition of the RLS is the minimum sum of the square error of the signal, and the optimal filtering process is achieved by estimating the parameters online and adaptively adjusting the parameters at the current moment to achieve the minimum-cost function. The minimum-cost function $P(t)$ is given by (20).

$$P(t) = \frac{P(t-1) - k(t)X^H P(t-1)}{\Delta} \tag{20}$$

Combined with $R$ and $E$, the IMFs can be divided into three categories: effective IMFs, noise IMFs, and aliasing IMFs. We proposed an RE-RLS-VMD information extraction method that preserves the effective IMFs, eliminates the noise IMFs, and uses RLS for secondary noise reduction of aliasing IMFs. This method can effectively extract effective information.

## IV. RE-RLS-VMD-DFNN DETECTION ALGORITHM

The residual current signal preprocessed by RE-RLS-VMD can significantly improve the SNR. Combining RE-RLS-VMD and DFNN, a new detection method called RE-RLS-VMD-DFNN was constructed, which can further improve the detection accuracy and operation speed. Taking the residual current signal of a single direct grounding fault occurring in a wetland environment as an example. The specific process is as follows:

1) According to the determined general $K$-value, the VMD decomposes the original residual current signal into five IMFs.
2) The cross-correlation coefficient $R$ and time-domain energy entropy ratio $E$ were calculated, and the IMFs were classified according to the values of $R$ and $E$.
3) The aliasing IMFs are secondarily noise reduced by RLS, and the denoised-aliasing IMFs are superimposed with the effective IMFs to obtain the reconstructed signal $x'(t)$.
4) The initial DFNN is trained with the reconstructed signal to obtain a neural network that can meet the actual detection accuracy requirements.
5) The reconstructed signal is processed by the trained DFNN to obtain the detection signal $y(t)$. The residual current can be predicted based on the detection signal [31].

The specific process is shown in Fig. 2.

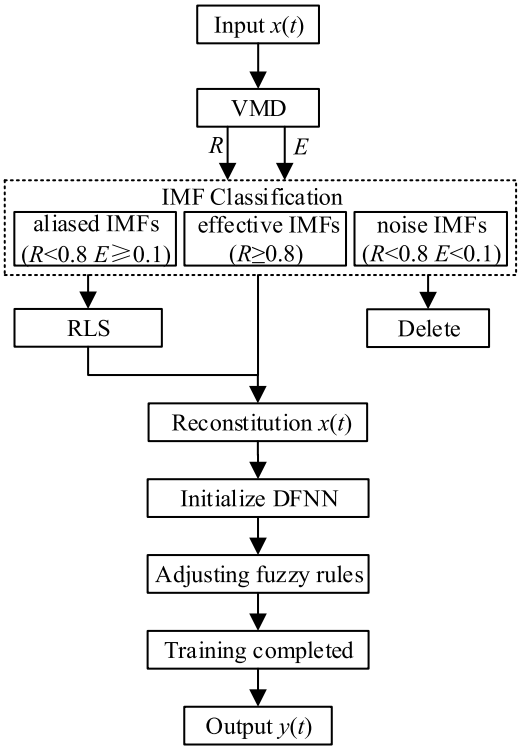


**FIGURE 2.** Flowchart of RE-RLS-VMD-DFNN.

## V. RE-RLS-VMD-DFNN DETECTION ALGORITHM

### A. SIMULATION EXPERIMENTS

To verify the effectiveness of the RE-RLS-VMD-DFNN, the equivalent circuit model of the H. Freiberger human body was constructed on the MATLAB/Simulink platform to conduct an electric shock simulation experiment on the human body [32]. The equivalent circuit is illustrated in Fig. 3.

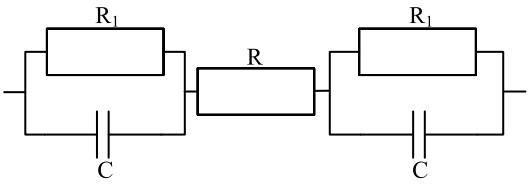


**FIGURE 3.** Equivalent circuit model of the human body.

According to the experimental results of H. Freiberg, when the voltage is 220 V, the skin impedance $R_1$ is 2000 Ω, the skin capacitance C is $2 \times 10^{-8}$ F, and the internal impedance R of the human body is 500 Ω. The analog voltage was set to 220 V, 50 Hz of single-phase AC, which was applied to the equivalent circuit to obtain the simulation signal of the residual current when the human body has an electric shock fault. To be more realistic, Gaussian white noise with SNR of 10 dB, 15 dB and 25 dB is added to the simulation signal, respectively.

#### 1) DENOISING PROCESS OF SIMULATION DATA

Taking the simulation signal with an SNR of 15 dB as an example, the simulation signal was preprocessed by RE-RLS-VMD. According to the proposed general $K$-value selection method, the general $K$-value of the human body electric shock residual current signal is 3. Therefore,

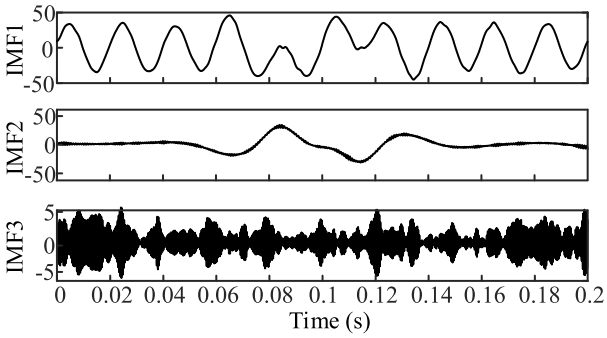


**FIGURE 4.** IMFs component.

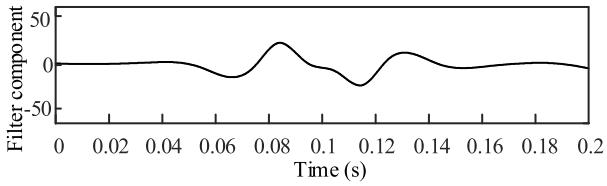


**FIGURE 5.** RLS filtering.

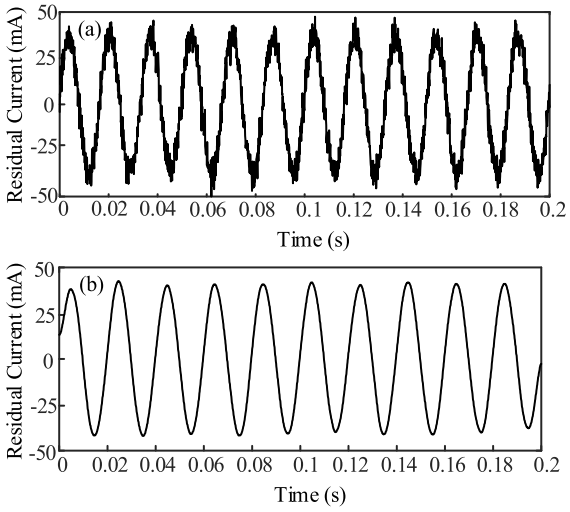


**FIGURE 6.** Simulated and reconstructed signals. (a) The simulated signal. (b) The reconstructed signal.

the VMD decomposes the signal into three IMFs, as shown in Fig. 4.

After calculating the classification indexes $R$ and $E$, the $R$ values of each IMF are 0.825, 0.237 and 0.074, respectively. The $E$ values of each IMF are 0.812, 0.156 and 0.032, respectively. According to the proposed classification method of IMFs, IMF1 is an effective IMF, IMF2 is an aliasing IMF, and IMF3 is the noise IMF. The aliasing IMF is denoised by RLS, where the order of the RLS filter is 3, the forgetting factor is 0.98, and the maximum error of iteration is 0.01. The aliasing IMF after RLS processing is shown in Fig. 5.

The denoised aliasing IMF and effective IMF are superimposed to obtain the reconstructed signal, as shown in Fig. 6(b).

It can be seen from Fig. 6 that the RE-RLS-VMD can reconstruct the signal well when the SNR is 15 dB. After calculation, $R$ between the reconstructed signal and the simulation signal was 0.925. To better reflect the superiority of the RE-RLS-VMD method, the simulation signals with SNR of 10 dB, 15 dB, and 25 dB are compared in terms of running time $t$ and mean square error (MSE) when the RE-RLS-VMD takes the general $K$-value and VMD takes the optimal $K$-value [33]. The comparison results are listed in Table 3.

**TABLE 3.** Comparison of VMD and RE-RLS-VMD.

| SNR | Indicators | Optimal *K-value* | General *K-value* |
|---|---|---|---|
| 10 | *t*/s | 0.9482 | 0.9846 |
| | MSE | 0.1864 | 0.1634 |
| 15 | *t*/s | 0.8569 | 0.8750 |
| | MSE | 0.1682 | 0.1478 |
| 25 | *t*/s | 0.7152 | 0.7467 |
| | MSE | 0.0973 | 0.0827 |

It can be seen from Table 3 that when the SNR is 10 dB, 15 dB and 25 dB, the MSE of RE-RLS-VMD are 12.3%, 12.1% and 15.0% lower than that of VMD, respectively. The $t$ of RE-RLS-VMD are 3.8%, 2.2% and 4.4% slightly longer those of VMD, respectively. Thus, the RE-RLS-VMD sacrifices a small amount of running time but further improves the accuracy of the reconstructed signal when dealing with the residual current signal with noise.

### 2) DFNN DETECTION

After RE-RLS-VMD processing, the effective components in the noisy signal are extracted. The reconstructed simulation signal was input into the trained DFNN for detection, and the residual current signal was predicted through the detection signal, as shown in Fig. 7.

As shown in Fig. 7, the residual current signal processed by RE-RLS-VMD has good detection results in the DFNN. After calculation, the $R$ between the actual signal and the detection signal is 0.9361, while the $R$ between the actual signal and the predicted signal is 0.8829, both of which can meet the requirements of RCD for residual current detection accuracy.

### 3) COMPARATIVE ANALYSIS OF ALGORITHMS

To further demonstrate the superiority of RE-RLS-VMD-DFNN, this method was compared with three newly proposed residual current detection methods: WNN, EMD-T, and WE-AE-BP. In different SNR environments, the detection results of different methods were compared with $t$, MSE and goodness of fit ($R^2$). Where closer $R^2$ is to 1, a better fit of the detection value is indicated. The comparison results of the four methods are presented in Table 4.

Table 4 shows that RE-RLS-VMD-DFNN is superior to WNN, EMD-T, and WE-AE-BP in t, MSE, and $R^2$ when detecting residual current under different SNR. Compared

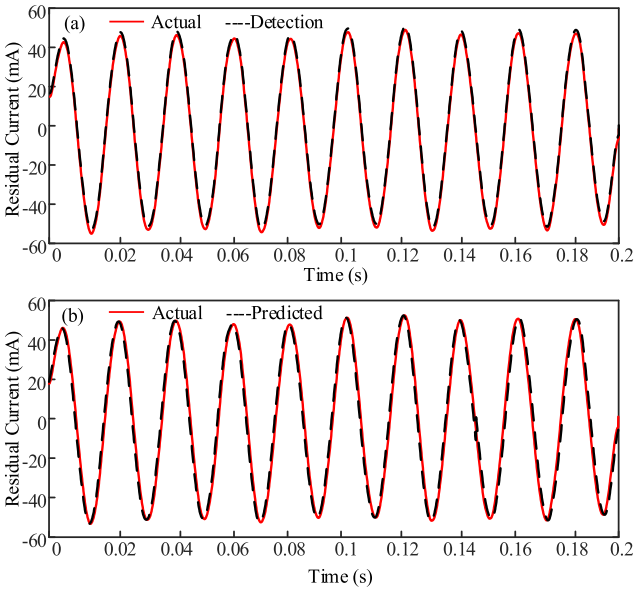


**FIGURE 7.** The residual current of human electric shock by DFNN. (a) Actual and detection signals. (b) Actual and predicted signals.

**TABLE 4.** Comparison of the detection results.

| SNR | Indicators | WNN | EMD-T | WE-AE-BP | RE-RLS-VMD-DFNN |
|---|---|---|---|---|---|
| 10 | *t/s* | 2.5696 | 2.3658 | 2.5314 | 2.1741 |
| | $R^2$ | 0.8530 | 0.8371 | 0.8745 | 0.8952 |
| | MSE | 0.4941 | 0.4250 | 0.4284 | 0.3508 |
| 15 | *t/s* | 2.4814 | 2.2981 | 2.2114 | 2.0203 |
| | $R^2$ | 0.8857 | 0.8613 | 0.8832 | 0.9261 |
| | MSE | 0.3846 | 0.3957 | 0.3527 | 0.3451 |
| 25 | *t/s* | 2.5237 | 2.4966 | 2.7515 | 2.2930 |
| | $R^2$ | 0.9076 | 0.8935 | 0.8933 | 0.9356 |
| | MSE | 0.3687 | 0.3751 | 0.3482 | 0.3296 |

with WNN, EMD-T and WE-AE-BP methods, the t of RE-RLS-VMD-DFNN decreased by 14.35%, 9.40% and 13.44%, respectively, the $R^2$ of RE-RLS-VMD-DFNN increased by 3.42 %, 5.59 % and 3.99 %, respectively, and the MSE of RE-RLS-VMD-DFNN decreased by 17.78%, 14.24% and 9.19%, respectively.

### *B. MEASURED DATA*

The residual current detection platform built in the laboratory was used to collect the residual current signals of various fault types. The experimental platform adopted a 220 V, 50 Hz single-phase AC. The sampling time of the experimental data is 0.5s, the fault starts at 0.1s and ends at 0.4s. The sampling frequency of the oscilloscope was 10 kHz, and effective data of 15 cycles were collected.

Residual current signals of common plant electric shocks and single direct grounding faults were collected in different environments. The residual current signals of the plant electric shock were measured in two environments: 1). Poplars with a diameter of 5 cm and height of about 2.5 m. 2). Shrub with a height of approximately 50 cm. A single direct grounding fault occurs in the concrete floor and wetland environments. The residual current signals of different fault types were collected using a Tektronix MOD3024 mixed-domain oscilloscope in high-resolution sampling mode. Twenty groups of data were collected for each type of fault. The residual current waveforms for the different fault types are shown in Fig. 8.

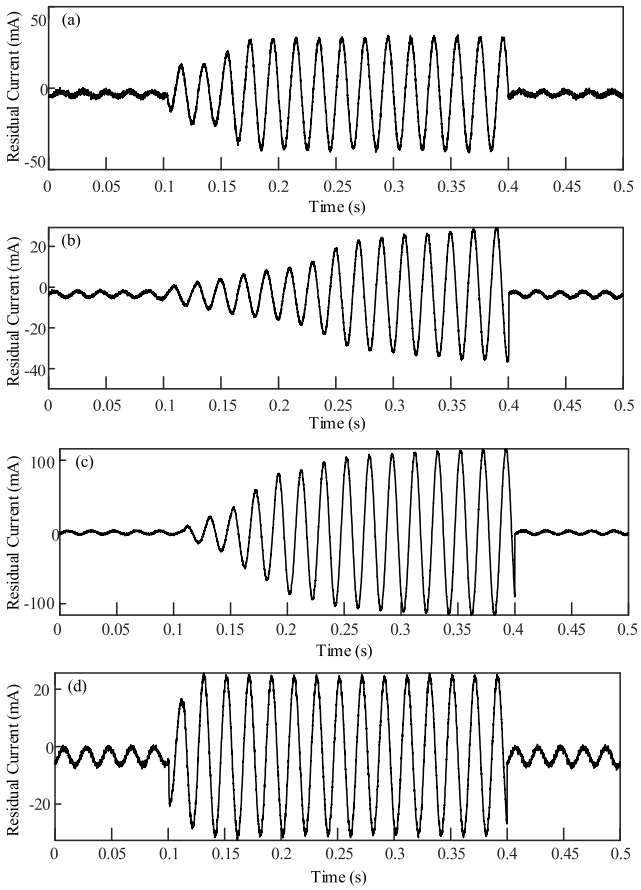


**FIGURE 8.** Different types of residual current measured signals. (a) Poplar. (b) Shrub. (c) Wetland. (d) Concrete floor.

#### 1) DENOISING PROCESS OF MEASURED DATA

Taking the residual current signal of a single direct grounding fault in a wetland environment as an example, Gaussian white noise with an SNR of 15 dB is added to the measured residual current signal, and the RE-RLS-VMD method was used for preprocessing. The IMF components of VMD decomposition are shown in Fig. 9.

After calculation, the *R* of the five IMFs component are: 0.9367, 0.2264, 0.1181, 0.0380, 0.0213, and the *E* are: 0.6342, 0.1218, 0.1047, 0.0562, 0.0120, respectively. According to the classification method of IMFs, IMF1 is the effective IMF, IMF2 and IMF3 were the aliasing IMFs. The superimposed signals of IMF2 and IMF3 are subjected to

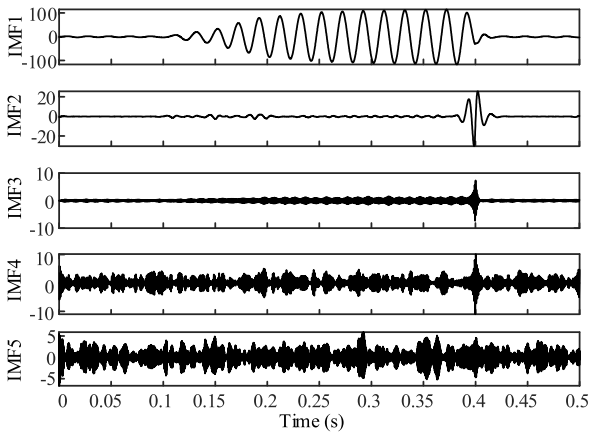


**FIGURE 9.** IMF components.

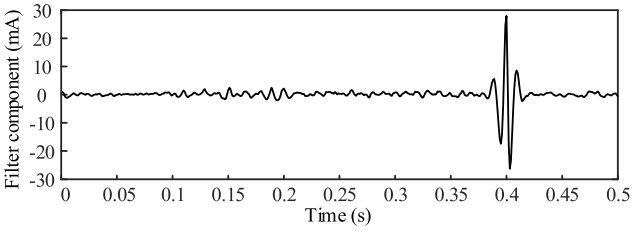


**FIGURE 10.** RLS filtering.

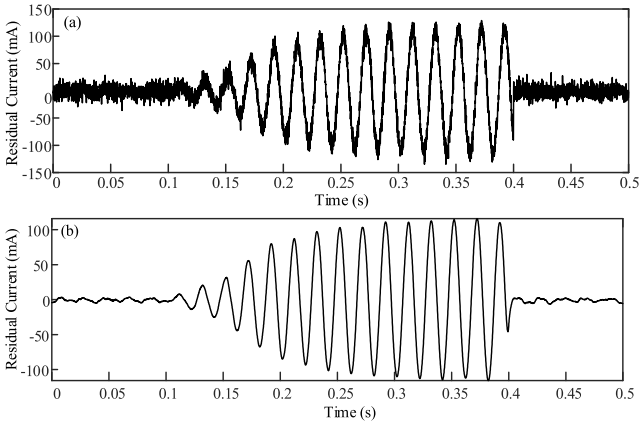


**FIGURE 11.** Measured and reconstructed signals. (a) Measured signal. (b) Reconstructed signal.

secondary noise reduction by RLS, and the results are shown in Fig. 10.

The effective IMF is superimposed with the denoised aliasing IMF to obtain the reconstructed signal. The measured and reconstructed signals are presented in Fig. 11.

From Fig. 11, most of the noise in the measured residual current signal preprocessed by RE-RLS-VMD was removed, and the effective information was accurately extracted. Table 5 shows the comparison of the measured signal preprocessing results when VMD takes the optimal $K$-value and RE-RLS-VMD takes the general $K$-value.

**TABLE 5.** Comparison of VMD and RE-RLS-VMD.

| SNR | Indicators | Optimal $K$-value | General $K$-value |
|---|---|---|---|
| 10 | $t$/s | 0.9897 | 1.0392 |
| | MSE | 0.2752 | 0.2464 |
| 15 | $t$/s | 0.8578 | 0.8851 |
| | MSE | 0.2741 | 0.2338 |
| 25 | $t$/s | 0.8461 | 0.8756 |
| | MSE | 0.2735 | 0.2264 |

Table 5 shows that the MSE of RE-RLS-VMD compared with VMD at SNR of 10dB, 15dB and 25dB is reduced by 10.5%, 14.7% and 17.2%, respectively. While the $t$ is slightly more than VMD, which are 4.76%, 3.08% and 3.37%, respectively. In comparison, the RE-RLS-VMD reduces the requirement of $K$ value and greatly improves the denoising effect at the expense of certain running time. Therefore, RE-RLS-VMD has higher adaptability under different SNR and is more suitable for the residual current signal preprocessing. Taking the fault signals with the SNR is 15dB as an example, the RE-RLS-VMD is used to denoise the fault signal. The denoising results for the residual current signals of the four fault types are shown in Figure 12.

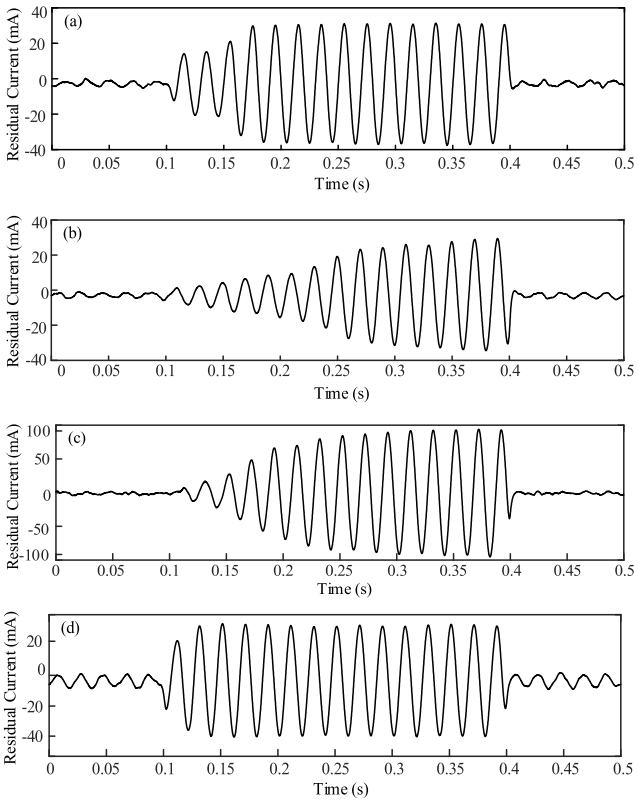


**FIGURE 12.** Reconstructed signal by RE-RLS-VMD. (a) Poplar. (b) Shrub. (c) Wetland. (d) Concrete floor.

As can be seen from Fig. 12, the measured residual current signals of the four fault types preprocessed by the RE-RLS-VMD method have been greatly recovered.

### 2) DFNN DETECTION

Taking the electric shock of poplar and single direct grounding in a wetland environment as an example. The residual current signal collected in the experiment had 15 effective cycles. After RE-RLS-VMD preprocessing, the measured signal with an SNR of 15 dB was input into the trained DFNN for detection, and the corresponding signal was predicted according to the detected signal. The detection and predicted signals for the electric shock of poplar and single direct grounding in a wetland environment fault types of residual currents are shown in Fig. 13 and Fig. 14, respectively.

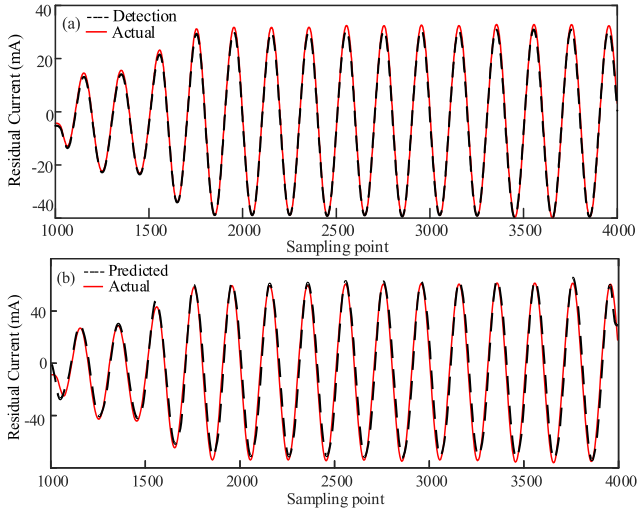


**FIGURE 13.** The residual current of plant electric shock by DFNN. (a) Detection and actual signals. (b) Predicted and actual signals.

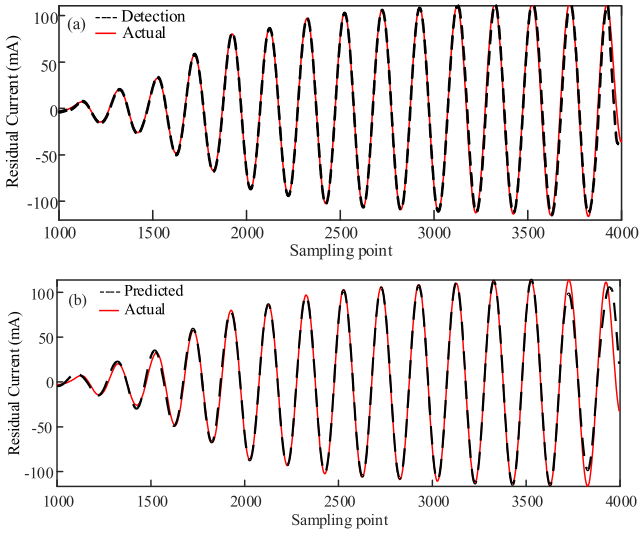


**FIGURE 14.** The residual current of single direct grounding fault by DFNN. (a) Detection and actual signals. (b) Predicted and actual signals.

From Fig. 13 and Fig. 14, it can be concluded that the RE-RLS-VMD-DFNN has high accuracy when detecting the residual current signals of the two fault types, and the detection errors are 5.38% and 3.92%, respectively. When the DFNN is used to predict the fault residual current signal, the prediction accuracies of the two fault types are 83.54% and 86.91% respectively, which can also meet the requirements of the RCD.

### 3) COMPARATIVE ANALYSIS OF ALGORITHMS

To demonstrate the advantages of RE-RLS-VMD-DFNN in residual current detection of measurement data, it was compared with WNN, EMD-T, and WE-AE-BP, and the comparison results are shown in Table 6.

**TABLE 6.** Comparison of the detection results.

| SNR | Indicators | WNN | EMD-T | WE-AE-BP | RE-RLS-VMD-DFNN |
|---|---|---|---|---|---|
| 10 | *t/s* | 2.7532 | 2.6324 | 2.7852 | 2.2785 |
| | $R^2$ | 0.8516 | 0.8367 | 0.8726 | 0.9067 |
| | MSE | 0.5483 | 0.5450 | 0.5316 | 0.5134 |
| 15 | *t/s* | 2.9058 | 2.5469 | 2.8631 | 2.3576 |
| | $R^2$ | 0.8942 | 0.8742 | 0.8834 | 0.9361 |
| | MSE | 0.5327 | 0.5952 | 0.5156 | 0.4988 |
| 25 | *t/s* | 2.8147 | 2.7706 | 2.9531 | 2.3270 |
| | $R^2$ | 0.9279 | 0.9184 | 0.9266 | 0.9568 |
| | MSE | 0.5259 | 0.5403 | 0.5053 | 0.4781 |

Table 6 shows that RE-RLS-VMD-DFNN is better than WNN, EMD-T and WE-AE-BP in terms of the $t$, $R^2$ and MSE under different SNR. By comparison, the EMD-T is better than WNN and WE-AE-BP in terms of $t$, while RE-RLS-VMD-DFNN is 12.41% faster than EMD-T. The WE-AE-BP is better than WNN and EMD-T in both $R^2$ and MSE, while in terms of $R^2$, the RE-RLS-VMD-DFN is 4.36 % higher than WE-AE-BP, and in terms of MSE, the RE-RLS-VMD-DFN is 4.01 % lower than WE-AE-BP. The detection results of the measured data also demonstrate the effectiveness of the RE-RLS-VMD-DFNN.

## VI. CONCLUSION

To solve the problem of residual current detection in low-voltage distribution networks, we proposed a residual current detection method based on RE-RLS-VMD and DFNN. First, in order to solve the problem that the $K$-value of VMD is difficult to determine when processing the residual current signal, we proposed the concept and determination method of general $K$-value, which reduces the operation time and operation volume compared with the method of seeking the optimal $K$-value. Second, in order to better extract the effective components in the residual current signal, we propose to classify the IMF by cross-correlation coefficients and time-domain energy entropy occupancy ratio, and extract the effective components in the aliasing IMFs by RLS, which

further improves the signal preprocessing capability of VMD. Finally, we used the DFNN constructed by the minimum output method to detect the preprocessed signals, which overcomes the shortcomings of the fixed structure of traditional neural networks and has high accuracy.

Compared with the residual current processed by EMD-T, the number of IMFs generated by VMD is controllable, which can avoid the shortcomings of EMD over-decomposition and mode aliasing due to noise. Compared with WNN and WE-AE-BP, the RE-RLS-VMD-DFNN does not need to adjust the parameters in advance, which maintains the effectiveness of the neural network during the detection process and overcomes the drawback that BPNN easily falls into a local minimum owing to improper structure and parameter settings. The simulation and measured data show that RE-RLS-VMD-DFNN is superior to the WNN, EMD-T, and WE-AE-BP methods in terms of running time $t$, goodness of fit $R^2$, and MSE. The RE-RLS-VMD-DFNN has a higher detection accuracy, and can be used in adaptive RCD to achieve an instantaneous response to leakage or electric shock accidents.

## ACKNOWLEDGMENT

The authors would like to thank Shandong Kehui Electric Company Ltd., for providing the experimental space and experimental equipment contribution in Zibo, Shandong, China.

## REFERENCES

[1] X. Han, S. Du, Z. Li, and L. Sun, "Diagnosis of electric shock fault based on time-frequency singular value spectrum of leakage current and fuzzy clustering," *Nongye Gongcheng Xuebao/Trans. Chin. Soc. Agricult. Eng.*, vol. 34, no. 4, pp. 217–222, 2018.

[2] H. Guan, "An automatic and quick detection model of electric shock signals," *Power Syst. Technol.*, vol. 37, no. 8, pp. 2328–2335, 2013.

[3] X. Han, W. Sheng, S. Du, J. Su, and G. Liu, "Novel protection scheme for residual current device-based electric fault time detection and touch current identification," *IET Gener., Transmiss. Distrib.*, vol. 11, no. 10, pp. 2478–2488, Jul. 2017.

[4] S. Czapp and H. Tariq, "Behavior of residual current devices at frequencies up to 50 kHz," *Energies*, vol. 14, no. 6, p. 1785, Mar. 2021.

[5] C. Li, H. Du, J. Su, Y. Xia, and J. Huang, "A novel detecting method of electric shock signal based on wavelet transform and chaotic theory," *Power Syst. Protection Control*, vol. 39, no. 10, pp. 47–52, 2011.

[6] J. Wang, Y. Liu, X. Han, S. Du, L. Wang, J. Su, G. Liu, and H. Guan, "Denoising of electrical shock fault signal based on empirical mode decomposition thresholding," in *Proc. China Int. Conf. Electr. Distrib. (CICED)*, Aug. 2016, pp. 1–5.

[7] H. Guan, W. Li, H. Du, C. Li, and L. Li, "Detection model of biological electric shock current based on Hilbert–Huang transform," *Trans. CSAE*, vol. 33, no. 14, pp. 202–209, 2017.

[8] C. Li, J. Su, H. Du, Y. Xia, J. Zhang, and L. Zhang, "Detecting model of electric shock signal based on wavelet analysis and BP neural network," *Trans. CSAE*, vol. 26, no. S2, pp. 130–134, 2010.

[9] S. Wu, S.-Y. Lin, and M.-F. Guo, "Application of WE-AE-BP method to electric shock faults identification in the low-voltage distribution network," in *Proc. IEEE 1st China Int. Youth Conf. Electr. Eng. (CIYCEE)*, Nov. 2020, pp. 1–6.

[10] X. Han, H. Du, J. Su, H. Guan, and L. Shao, "Determination method of electric shock current based on parameter-optimized least squares support vector machine," *Trans. CSAE*, vol. 30, no. 23, pp. 238–245, 2014.

[11] A. O. Boudraa and J. C. Cexus, "EMD-based signal filtering," *IEEE Trans. Instrum. Meas.*, vol. 56, no. 6, pp. 2196–2202, Dec. 2007.

[12] P. M. R. Bento, J. A. N. Pombo, M. R. A. Calado, and S. J. P. S. Mariano, "A bat optimized neural network and wavelet transform approach for short-term price forecasting," *Appl. Energy.*, vol. 210, pp. 88–97, Jan. 2018.

[13] L. Sun, L. Su, and J. Wang, "Non-fragile dissipative state estimation for semi-Markov jump inertial neural networks with reaction-diffusion," *Appl. Math. Comput.*, vol. 411, Dec. 2021, Art. no. 126404.

[14] J. Wang, X. Wang, N. Xie, J. Xia, and H. Shen, "Fuzzy-model-based $\mathcal{H}_\infty$ pinning synchronization for coupled neural networks subject to reaction-diffusion," *IEEE Trans. Fuzzy Syst.*, early access, Nov. 9, 2020, doi: 10.1109/TFUZZ.2020.3036697.

[15] J. Wang, J. Xia, H. Shen, M. Xing, and J. H. Park, "$\mathcal{H}_\infty$ synchronization for fuzzy Markov jump chaotic systems with piecewise-constant transition probabilities subject to PDT switching rule," *IEEE Trans. Fuzzy Syst.*, vol. 29, no. 10, pp. 3082–3092, Oct. 2021.

[16] J. Wei, T. Xie, M. Shi, Q. He, T. Wang, and Y. Amirat, "Imbalance fault classification based on VMD denoising and S-LDA for variable-speed marine current turbine," *J. Mar. Sci. Eng.*, vol. 9, no. 3, p. 248, Feb. 2021.

[17] Y. Meng, T. Liu, K. Liu, J. Jiang, R. Wang, T. Wang, and H. Hu, "A modified empirical mode decomposition algorithm in TDLAS for gas detection," *IEEE Photon. J.*, vol. 6, no. 6, pp. 1–7, Dec. 2014.

[18] O. Fasil and R. Rajesh, "Time-domain exponential energy for epileptic EEG signal classification," *Neurosci. Lett.*, vol. 694, pp. 1–8, Feb. 2019.

[19] D. Wang, X. Xu, T. Zhang, Y. Zhu, and J. Tong, "An EMD-MRLS denoising method for fiber optic gyro signal," *Optik*, vol. 183, pp. 971–987, Apr. 2019.

[20] X. Ma, Y. Jin, and Q. Dong, "A generalized dynamic fuzzy neural network based on singular spectrum analysis optimized by brain storm optimization for short-term wind speed forecasting," *Appl. Soft. Comput.*, vol. 54, pp. 296–312, May 2017.

[21] A. T. Jahromi, M. J. Er, X. Li, and B. S. Lim, "Sequential fuzzy clustering based dynamic fuzzy neural network for fault diagnosis and prognosis," *Neurocomputing*, vol. 196, pp. 31–41, Jul. 2016.

[22] K. Dragomiretskiy and D. Zosso, "Variational mode decomposition," *IEEE Trans. Signal Process.*, vol. 62, no. 3, pp. 531–544, Feb. 2014.

[23] P. D. Achlerkar, S. R. Samantaray, and M. S. Manikandan, "Variational mode decomposition and decision tree based detection and classification of power quality disturbances in grid-connected distributed generation system," *IEEE Trans. Smart Grid*, vol. 9, no. 4, pp. 3122–3132, Jul. 2018.

[24] S. Li, C. Xia, Z. Cheng, W. Mao, Y. Liu, and D. Habibi, "Leak location based on PDS-VMD of leakage-induced vibration signal under low SNR in water-supply pipelines," *IEEE Access*, vol. 8, pp. 68091–68102, 2020.

[25] X. Chen, Z. Yang, and W. Lou, "Fault diagnosis of rolling bearing based on the permutation entropy of VMD and decision tree," in *Proc. 3rd Int. Conf. Electron. Inf. Technol. Comput. Eng. (EITCE)*, Oct. 2019, pp. 1911–1915.

[26] J. Zhang and J. Wu, "A new feature extraction for rolling bearing using sparse representation based on improved K-singular value decomposition and VMD," in *Proc. 7th Int. Conf. Condition Monitor. Machinery Non-Stationary Oper. (CMMNO)*, Jun. 2021, pp. 27–31.

[27] Y. Shi, Y. Wang, Y. Mei, and S. Liu, "VMD harmonic detection method based on WPT snd parameter optimization," *Electr. Meas. Instrum.*, pp. 1–6, Jul. 2020. [Online]. Available: http://kns.cnki.net/kcms/detail/23.1202.TH.20200713.1107.010.html

[28] Q. Ge, G. Zhang, and X. Zhang, "Automatic detection of epilepsy based on EMD-VMD feature components and ReliefF algorithm," in *Proc. 11th Int. Conf. Inf. Sci. Technol. (ICIST)*, May 2021, pp. 87–93.

[29] J. Ding, D. Xiao, and X. Li, "Gear fault diagnosis based on genetic mutation particle swarm optimization VMD and probabilistic neural network algorithm," *IEEE Access*, vol. 8, pp. 18456–18474, 2020.

[30] S. Olyaee, M. S. E. Abadi, S. Hamedi, and F. Finizadeh, "Use of adaptive RLS, LMS, and NLMS algorithms for nonlinearity modeling in a modified laser interferometer," *Frontiers Optoelectron. China*, vol. 3, no. 3, pp. 264–269, Sep. 2010.

[31] S. Du, M. Wu, L. Chen, and W. Pedrycz, "Prediction model of burn-through point with fuzzy time series for iron ore sintering process," *Eng. Appl. Artif. Intell.*, vol. 102, Jun. 2021, Art. no. 104259.

[32] D. J. Bora and R. Dasgupta, "Estimation of skin impedance models with experimental data and a proposed model for human skin impedance," *IET Syst. Biol.*, vol. 14, no. 5, pp. 230–240, Oct. 2020.

[33] N. Halay and K. Todros, "MSE based optimization of the measure-transformed MUSIC algorithm," *Signal Process.*, vol. 160, pp. 150–163, Jul. 2019.

**XIANGKE ZHANG** was born in Tai'an, Shandong, China, in 1997. He received the B.E. degree from Linyi University, Linyi, China, in 2020. He is currently pursuing the M.E. degree with the Shandong University of Technology, Zibo, China. His research interest includes electrical measurement technology and application.

**ZHENMING LIU** was born in Qingzhou, Shandong, China, in 1994. He received the B.E. degree from the Shandong University of Technology, Zibo, China, in 2017, where he is currently pursuing the M.E. degree. His research interest includes weak signal detection technology.

**YAJING WANG** was born in Hebei, China, in 1971. She received the B.E. degree from Shandong Jianzhu University, in 1993, the M.E. degree from the Shandong University of Science and Technology, in 2000, and the Ph.D. degree from the Shanghai University of Science and Technology, in 2011.

She is currently a Professor with the College of Electrical and Electronic Engineering, Shandong University of Technology. She is also the Director of the Department of Electronic Information and a Ph.D. Supervisor. She has hosted and participated in more than 30 projects. She has published more than 80 articles in authoritative academic publications, many of which have been cited by international peers. Her main research interests include power quality analysis, weak signal detection technology, and intelligent signal processing technology.

**ZHENHAI DOU** was born in Beijing, China, in 1970. He received the M.E. degree in electrical engineering from the Inner Mongolia University of Science and Technology (IMUST), China, in 2005, and the D.E. degree in electrical engineering from China Agricultural University (CAU), Beijing, in 2014.

Since 2013, he has been an Associate Professor with the School of Electrical and Electronic Engineering, Shandong University of Technology (SDUT), Shandong, China. He is currently the Head of the Department of Electrical Engineering, SDUT. His research interests include power system load forecasting and power system automation.

**GUOLIANG ZHAI** was born in Jining, Shandong, China, in 1996. He received the B.E. degree from the Qilu University of Technology, Jinan, China, in 2020. He is currently pursuing the M.E. degree with the Shandong University of Technology, Zibo, China. His research interest includes intelligent distribution network automation technology and application.

**QINQIN WEI** was born in Zibo, Shandong, China, in 1980. She received the B.E. degree, in 2001, the M.S. degree, in 2004, and the Ph.D. degree from Peking University, Beijing, China, in 2012. She is currently a Teacher at the College of Electrical and Electronic Engineering, Shandong University of Science and Technology. Her research interests include carbonkina electronic materials and devices.